Universitat Politècnica de Catalunya

Treball Final del Grau en Enginyeria Física

Study of the Effect of Viscosity in Drop Breakup in Turbulent Flows.

CENTER OF
APPLIED SPACE TECHNOLOGY
AND MICROGRAVITY

ZARM - University of Bremen

June 2021

Author: Lucas Fernandez Stolpa

Director: Prof. Dr. Marc Avila

Codirector: Dr. Alvaro Meseguer

Supervisor: Dr. Alberto Vela-Martín

Acknowledgements

I would like to express my gratitude to Prof. Dr. Marc Avila, who accepted me to join the Zentrum für angewandte Raumfahrttechnologie und Mikrogravitation (ZARM) at the University of Bremen and proposed me the topic of drop breakup.

Also, I would really like to thank Dr. Alberto Vela-Martín, who supervised my work and besides always being available to help me, he kept me motivated and focused on the objectives during the development of the work.

Finally, I want to thank my co-director Dr. Alvaro Meseguer at the Universitat Politècnica de Catalunya. His lectures on Fluids and Computational Methods motivated me to choose the subject of my bachelor thesis and helped me to contact Prof. Avila.

Notation Dictionary

t time

x_i cartesian coordinate

u_i velocity

ρ density

p hydrostatic pressure

μ dynamic viscosity

ν kinematic viscosity

Re Reynolds number

We Weber number

τ_{ij} stress tensor

σ surface tension

ω_i vorticity

Ω enstrophy

S_{ij} rate-of-strain tensor

ε dissipation rate

η Kolmogorov length scale

A_{ij} velocity gradient tensor

W_{ij} rate-of-rotation tensor

Q second invariant

R third invariant

Contents

Abstract

The systems formed by two immiscible liquids such as emulsions are of great interest in industrial processes, the emulsion formation process occurs depending on the phenomenon of the breakup of the drops of one of the fluids within the other, and the properties depend on how this phenomenon happens. The breakup of drops in turbulent flows is investigated to determine which mechanisms are those that interact in the breakup and what is the effect of the viscosity of the drop on the dynamics of the break. For this study we used the data generated in the simulations of the work "Energetics of drop deformation with application to turbulence" [1], to make an analysis of the average behavior of the velocity gradients, comparing one hundred simulations with different initial conditions, to identify the mechanisms as mentioned previously. In a first analysis we show the importance of the distance with respect to the interface of the drop in terms of the influence that the dynamics of the surface has on the rest of the flow. The main analysis of the work uses tensor invariants to observe how the mechanisms that regulate the dynamics of the breakup interact and change with viscosity.

1 Introduction

1.1 Motivation

Gas-liquid or liquid-liquid mixtures, emulsions and dispersions, are of great relevance in industries such as chemical, oil, pharmaceutical and mining. The phenomenon of droplet or bubble breaking is found in a wide variety of processes such as mixing, extraction, absorption, chemical reactions, food industry, water and water treatment, pharmaceutical synthesis or various other operations in the chemical processing industry. To create these systems, at least two immiscible liquids must be agitated turbulently to generate a dispersive flow that ensures good contact between the phases and allows control of the interficial area. The latter is crucial to achieve rapid heating and mass transfer between phases [2].

The knowledge of the parameters that can affect the dynamics of the breaking of drops and bubbles (fluid particles) in dispersive systems is a topic of great relevance in mixing processes. Understanding drop deformation in turbulent flows is therefore a key process in many natural phenomena that also take place in industrial applications. A better understanding of the mechanisms that drives this breakup process is key for developing models that can predict how and when the breakup occurs.

The objectives that we established for the development of the work and that ideally should be followed are:

1. First approach to the concept of turbulent flows, forming structures such as eddies and related concepts such as vortex stretching.

2. Understand the model of drop breakup used in the simulation of the data being analyzed.

3. First analysis of the velocity gradients to observe how they change in the simulation cube.

4. In-depth study of the flow dynamics from the invariants of the velocity gradient tensor to identify the main mechanisms that interact in the breakup by varying the viscosity of the drop.

1.2 Fundamentals of drop breakup

The conceptual basis of the breakup of a drop immersed in a turbulent flow, forming a system of two fluid phases, includes the analysis of the local viscous effects in the breakup of drops smaller than the Kolmogorov scale and the inertial effects in the breakup of drops larger than the Kolmogorov microscale.

The deformation of the drop prior to its breakup is caused by continuous interactions with turbulent eddies, the drop responds to these interactions by making changes in its shape in a oscillatory behavior between stable and unstable structures and the drop breaks when the deformation reaches a critical value.

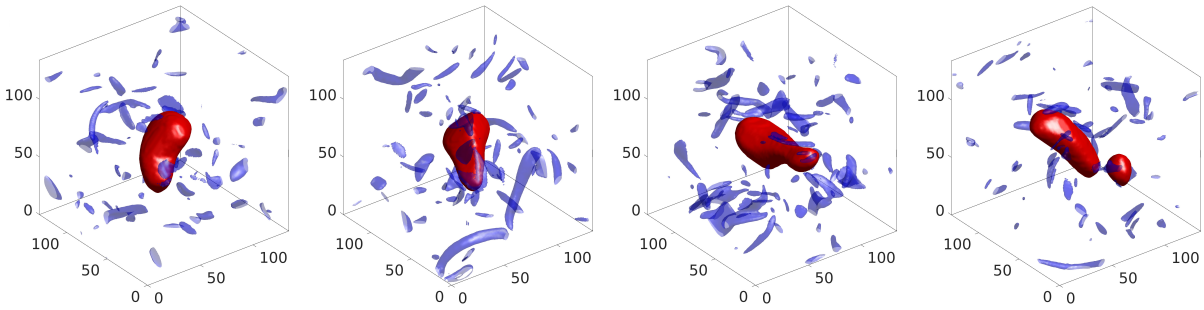

Figure 2: Temporal evolution of a drop at $We = 1.8$. The frame is fixed at the center of the drop, and the snapshots correspond consecutive time instants until the drop breakup. In red the drop and the blue isosurfaces denote regions of intense vorticity. The size of the computational box is marked in Kolmogorov units.

The breakup of a structure occurs where two fluids or a fluid in a vacuum form a free surface with a certain surface energy. If there is more surface area in the system than the minimum required to contain the volume of fluid, the system has an excess of surface energy. When the system is not in a state of minimum energy it tries to reorganize itself to return to the state of minimum energy which leads to the breakup of the fluid structure as such in smaller and separate structures to minimize the energy of the surface of the system having reduced the surface area.

The exact process of breaking depends on more mechanisms than surface tension such as viscosity, density or the diameter of the droplet that is broken.

In a later section, the model chosen for the simulations that generate the data used in our work is explained. At the moment, it should be noted that the flow of the simulation cube is a homogeneous and isotropic turbulent flow, which implies that the properties of the flow are invariant with respect to translation and rotation, respectively. This means that it does not matter in which position of the cube with respect to the walls the drop is or the orientation of the drop in the flow, the physics and the consequences are the same as far as this is concerned.

1.3 Experiments on drop breakup

Experimental investigations of individual drop breakup are crucial to develop a description of the breakup in addition to verifying that the already developed models adjust to real experience or what changes are necessary to achieve a better model.

Over the years, there have been numerous studies that have investigated the breakup of fluid particles (droplets or bubbles) in turbulent conditions [3, 4, 5]. These investigations make use of different techniques and methods to characterize the phenomenon of breakup. Therefore, they have reached different conclusions regarding different mechanisms and the effect of operating parameters.

Lately there has been more publication of experimental research on individual droplets due to a significant improvement in experimental techniques and in the acquisition of image data. Hasan [6] conducts a review of experimental studies of individual drop and

bubble breakup in stirred tanks. The reviewed studies are aimed at quantifying the breakup time, the number and size of the fragments after breakup. This data is then correlated with flow conditions, fluid properties, and mother drop size. However, there is still a significant limitation of experimental techniques to spatially and temporally resolve micron-scale drop events that occur on a timescale of less than one millisecond. The available results in the breaking of individual drops is in the range of $0.26 - 6$ mm. These droplets are relatively large for liquid-liquid emulsions in fields such as food, cosmetics or oil recovery, where micron-scale droplets and less are desired to ensure emulsion stability.

The investigations reviewed by Hasan are related to two main aspects, the first refers to the surface and interface phenomena related to the breaking mechanism and the second to the effect that different operating parameters have on the phenomenon. Although investigations have provided important information, they have not been able to precisely characterize the breaking rate and the phenomenon of the particle breaking surface. Recently, due to the use of high-speed cameras and high-feature capture, they have led to a deeper understanding of the phenomenon of breakup, especially for concepts related to the mechanism and behavior of the surface. However, a comprehensive characterization of the breakup phenomenon is still in its early stages and there are many challenges to overcome in order to understand the mechanism.

Greater efforts are needed to investigate the breakup phenomenon using high-speed cameras with high technical skills to gain greater depth in the parameters related to the breakup mechanism and the effect of operating conditions.

1.4 Direct Numerical Simulations (DNS)

A new chapter in turbulence theory began in 1972: Orszag and Patterson demonstrated that it is possible to perform fully developed turbulent flow computational simulations. These simulations do not need a model to work, instead they simulate every eddy, from largest to smallest, is computable. Starting with initial conditions of the Navier-Stokes equation, it is integrated forward in time for a specified domain. It is like conducting an experiment, but on the computer rather than in a wind tunnel. So these simulations are called *numerical experiments* [7].

The potential benefits are thus immediately clear. The initial conditions can be controlled in the simulations in such a way that it is not possible in the laboratory. Furthermore, the amount of data that can be retrieved is overwhelming: in fact, the full history of the speed field $\mathbf{u}(\mathbf{x}, t)$ is available for inspection.

However, there was and is a but. When the Reynolds number Re is large, which is always the case, η is small. From the Kolmogorov scale $\eta = (\nu^3/\varepsilon)^{1/4}$ it is possible to estimate the number of points needed to calculate $\mathbf{u}$ and solve all eddy in turbulence. The spatial separation of the sample points, Δx, cannot be much greater than the Kolmogorov length η. The number of points that contain data required for any instant of a three-dimensional simulation is therefore

$$N_x^3 \sim \left(\frac{L_{BOX}}{\Delta x}\right)^3 \sim \left(\frac{L_{BOX}}{l}\right)^3 Re^{9/4} \tag{1.1}$$

Where N_x is the number of network points (or Fourier modes) in any direction and L_{BOX}

is a typical linear dimension of the computational domain. We can rewrite the above equation as

$$Re \sim \left(\frac{l}{L_{BOX}}\right)^{4/3} N_x^{4/3} \tag{1.2}$$

So you can immediately see that there is a problem. To obtain data with a large Reynolds number we need a large number of data points. Following the same reasoning it is found that the number of computational operations required for a simulation is approximately proportional to

$$\text{Computer time} \sim N_x^3 N_t \sim \left(\frac{T}{l/u}\right)\left(\frac{L_{BOX}}{l}\right)^3 Re^3 \tag{1.3}$$

Therefore, it is observed that in order to increase the value of Re, the researchers have generally opted for the simplest possible geometries. Those interested in homogeneous turbulence, as is the case study, usually choose the so-called triple-periodic cube. This does not represent a real physical problem well, but like $L_{BOX} \gg l$, so the bulk of the turbulence is not affected by boundary conditions. The great advantage of the periodic cube is that it allows particularly efficient numerical algorithms to solve the Navier-Stokes equations, the so-called pseudo-spectral methods, which have been implemented in the code of the simulations from which the analyzed data comes from. When periodicity is imposed in all three directions, the turbulence is necessarily homogeneous and solid boundaries cannot be included in the simulation.

2 Theoretical Background

2.1 Introduction to turbulence and vorticity dynamics

In recent times, more and more studies are focused on the study of velocity gradients in turbulent flows because they contain all the necessary information regarding rate of rotation, stretching and angular deformation of infinitesimal material lines, surfaces and volumes in fluid flows. Understanding these phenomena is key for elucidating the properties and dynamics of different mechanisms in turbulent flows such as the dissipation of kinetic energy on small scales, the generation and evolution of intense vorticity filaments due to vortex stretching.

In order to understand the topic of turbulence and the magnitudes inspected in this work it is necessary to begin with the basic equations of fluid dynamics to then be able to understand the posterior analysis [7, 8, 9].

Suppose we have a incompressible and Newtonian fluid with constant density ρ and constant viscosity μ. Its motion is given by the Navier-Stokes equations

$$\frac{D\vec{u}}{Dt} = -\frac{\vec{\nabla} p}{\rho} + \nu \nabla^2 \vec{u} \tag{2.1}$$

where ν is the kinematic viscosity $\nu = \mu/\rho$, equation 2.1 can be also written using the shear stress tensor as

$$\rho \frac{D\vec{u}}{Dt} = -\vec{\nabla} p + \frac{\partial \tau_{ij}}{\partial x_j} \tag{2.2}$$

the changed element of the equality represents the viscous forces. We can now relate this variable called the stress tensor τ_{ij} to the rate-of-deformation of fluid elements. Most of them obey Newton's law of viscosity, which states

$$\tau_{ij} \;=\; \rho\nu \left\{ \frac{\partial u_i}{\partial x_j} + \frac{\partial u_j}{\partial x_i} \right\}. \tag{2.3}$$

It is now convenient to introduce the rate-of-strain tensor as the quantity

$$S_{ij} \;=\; \frac{1}{2} \left[\frac{\partial u_i}{\partial x_j} + \frac{\partial u_j}{\partial x_i} \right] \tag{2.4}$$

and so the most compact form of Newton's law of viscosity can be written using the relation between the stress and rate-of-strain tensor as

$$\tau_{ij} = 2\,\rho\nu\, S_{ij}. \tag{2.5}$$

We now want to know the rate of work done by these viscous forces or dissipation of energy in a viscous fluid. Suppose we have a volume V of fluid whose boundary ζ is subject to viscous stresses $2\,\rho\nu\, S_{ij}$ then the rate of work on the fluid is given by

$$\dot{W} = \oint u_i(\tau_{ij} d\zeta_j) \tag{2.6}$$

from Gauss's theorem we may rewrite $\dot{W}$ as

$$\dot{W} = \int \frac{\partial}{\partial x_j}[u_i \tau_{ij}] dV \tag{2.7}$$

and so we conclude that the rate of work of τ_{ij} per unit volume is

$$\frac{\partial}{\partial x_j}[u_i \tau_{ij}] \;=\; \frac{\partial \tau_{ij}}{\partial x_j} u_i + \tau_{ij} \frac{\partial u_i}{\partial x_j} \tag{2.8}$$

the net viscous forces can be related to the first appearing term since $f_i = \partial \tau_{ij}/\partial x_i$, the second term can be rewritten as:

$$\tau_{ij} \frac{\partial u_i}{\partial x_j} \;=\; \frac{1}{2}[\tau_{ij} + \tau_{ji}] \frac{\partial u_i}{\partial x_j} \;=\; \frac{1}{2} \left[\tau_{ij} \frac{\partial u_i}{\partial x_j} + \tau_{ji} \frac{\partial u_j}{\partial x_i} \right] \;=\; \tau_{ij} S_{ij} \tag{2.9}$$

since $\tau_{ij} = \tau_{ji}$ because of symmetry, the rate of work on the fluid is

$$\frac{\partial [u_i \tau_{ij}]}{\partial x_j} \;=\; f_i u_i + \tau_{ij} S_{ij} \; . \tag{2.10}$$

The two contributions on the right represent changes in the energy of the fluid, as they must. However, they corresponding to two rather different processes. The first term is the rate of work of the net viscous force acting on a fluid element. This necessarily represents the rate of change of mechanical energy of the fluid. The second term must, therefore, correspond to the rate of change of internal energy (per unit volume) of the fluid. Thus we conclude that the rate of increase of internal energy per unit mass is

$$\varepsilon \;=\; \tau_{ij} S_{ij} / \rho \;=\; 2\nu S_{ij} S_{ij}. \tag{2.11}$$

The next concept to introduce is the vorticity which is defined as $\vec{\omega} = \vec{\nabla} \times \vec{u}$, and $\omega_i \omega_i / 2$ is called the enstrophy Ω. The reason why so much attention is paid to ω is that it is determined by the evolution equation which is simpler than the Navier-Stokes equation and is derived from it. Unlike u, ω cannot be created or destroyed inside a fluid (unless there are body forces, such as buoyancy) and is carried by the field of flow by familiar processes such as advection and diffusion. Also, localized distributions of ω remain localized, which is not the case for the velocity field. Therefore, when we speak of "eddy" in a turbulent flow we are referring to a vorticity blob and its associated rotational and irrotational motion.

The vorticity field $\boldsymbol{\omega}(\boldsymbol{x}, t)$ can be shown to be twice the intrinsic angular velocity $\boldsymbol{\Theta}$, of a small blob of fluid located at $\boldsymbol{x}$ at time t:

$$\boldsymbol{\omega} \;=\; 2\boldsymbol{\Theta} \tag{2.12}$$

$\boldsymbol{\omega}$ is a measure of the local (or intrinsic) rotation, or spin, of fluids elements. Note that the velocity gradients, $\partial u_i / \partial x_j$, at any one point can always be decomposed into a combination of strain and vorticity

$$\frac{\partial u_i}{\partial x_j} \;=\; \frac{1}{2} \left(\frac{\partial u_i}{\partial x_j} + \frac{\partial u_j}{\partial x_i} \right) + \frac{1}{2} \left(\frac{\partial u_i}{\partial x_j} - \frac{\partial u_j}{\partial x_i} \right) \;=\; S_{ij} - \frac{1}{2} \varepsilon_{ijk} \omega_k \tag{2.13}$$

The symbol ε_{ijk} is the Levy-Civita symbol which equals 1 if (i, j, k) is an even permutation of $(1, 2, 3)$, -1 if it is an odd permutation, and 0 if any index is repeated.

Although S_{ij} and ω_i represent different processes, one measuring the distortion rate of fluid elements and the other representing the rotation rate, S_{ij} and ω_i are not independent. This is exemplified by the relationship of each through the Laplacian of the velocity field.

$$\nabla^2 u_i \;=\; 2\frac{\partial S_{ij}}{\partial x_j} \;=\; -[\nabla \times \boldsymbol{\omega}]_i \tag{2.14}$$

We are now going to derive the governing vorticity equation. Let's start by rewriting the Navier-Stokes equation (2.1),

$$\frac{\partial \boldsymbol{u}}{\partial t} \;=\; \boldsymbol{u} \times \boldsymbol{\omega} - \nabla C + \nu \nabla^2 \boldsymbol{u} \tag{2.15}$$

where C is the Bernoulli function. After this we apply the curl to the equation 2.15 which results in an equation for ω:

$$\frac{\partial \boldsymbol{\omega}}{\partial t} \;=\; \nabla \times [\boldsymbol{u} \times \boldsymbol{\omega}] + \nu \nabla^2 \boldsymbol{\omega} \tag{2.16}$$

Which is usually written in its alternate form

$$\frac{D\boldsymbol{\omega}}{Dt} \;=\; (\boldsymbol{\omega} \cdot \nabla)\boldsymbol{u} + \nu \nabla^2 \boldsymbol{\omega}\;. \tag{2.17}$$

Observing the resulting equation it appears that the terms on the right represent: (i) the change in the moment of inertia of a fluid element due to the stretching of that element; and (ii) the viscous torque on the element. In short, the vorticity of a fluid blob can change because the blob is stretched, causing a change in the moment of inertia, or the other way is because the blob is rotated or slowed down by viscous stresses.

Next, we want to explore in particular the evolution of vortex stretching (i.e. enstrophy production). Our starting point is the vorticity equation 2.17 from which we can obtain an equation for the enstrophy,

$$\frac{D}{Dt}\left(\frac{\omega^2}{2}\right) \;=\; \omega_i \omega_j S_{ij} - \nu(\nabla \times \boldsymbol{\omega})^2 + \nabla \cdot [\nu \boldsymbol{\omega} \times (\nabla \times \boldsymbol{\omega})] \tag{2.18}$$

For simplicity, we consider the case of freely decaying turbulence (without average velocity) which is statistically homogeneous. So, taking averages, the divergence on the left disappears since $\langle\sim\rangle$ commutes with $\nabla \cdot [\sim]$ and $\nabla \cdot [\langle\sim\rangle] = 0$ because both are linear operators. The same is true for the term $\boldsymbol{u} \cdot \nabla(\omega^2/2) = \nabla \cdot (\omega^2 \boldsymbol{u}/2)$. So we are left with

$$\frac{\partial}{\partial t}\langle \boldsymbol{\omega}^2/2 \rangle \;=\; \langle \omega_i \omega_j S_{ij} \rangle - \nu \langle (\nabla \times \boldsymbol{\omega})^2 \rangle \tag{2.19}$$

The equation 2.19 tells us that enstrophy can be created or destroyed by the strain field, and it is destroyed by viscous forces.

In addition, two things need to be highlighted: (i) The stretching of the vorticity overweight the compression of the vortex lines so that the net effect of the strain field is to create enstrophy, i.e. $\langle \omega_i \omega_j S_{ij} \rangle$ is positive; and (ii) there is a balance between the enstrophy production and the viscous dissipation [7].

2.2 The Weber number

The Weber number is a characteristic parameter used in fluid dynamics, it is a dimensionless quantity that describes the relationship between the deforming inertial forces and the stabilizing cohesive forces for fluids that flow through a fluid medium, i.e., surface tension forces.

When a liquid flows through a second fluid phase (gas or liquid), then the fluid-mechanical or aerodynamic force causes the drop to deform and eventually disperse. The cohesion force associated with the surface tension or interfacial tension (σ) opposes the increase of the surface area that is caused by the deformation of the drop. Therefore, the drop is kept together by the surface or interfacial tension.

The Weber number expresses the relationship between the deforming inertial forces and stabilizing cohesive forces associated with the surface tension or interfacial tension as

$$We = \frac{\text{Inertial Force}}{\text{Cohesion Force}} = \frac{\rho\, v^2\, l}{\sigma} = \frac{\rho \varepsilon^{2/3} d^{5/3}}{\sigma} \tag{2.20}$$

where ρ is the density of the fluid, l the characteristic length and v the characteristic velocity for which we take the Kolmogorov scales for the length and velocity. We end up with the expression depending on the energy dissipation rate ε and the size of the drop d. If the Weber number is too large, the inertial forces outweigh the surface tension forces, to the point where the drop breaks into even smaller drops.

2.3 Description of the problem

2.3.1 Model of the drop breakup

The base of the model of the simulations of single drop breakup is the exchange of energy between the turbulent flux in which the drop is immerse and the surface energy of the drop. The magnitudes that characterize these concepts are known as turbulent kinetic energy (K_t) and surface energy (E_σ)

$$K_t = \frac{1}{2}\rho u^2 \sim \frac{1}{2}\rho u_d^2 d^3 \tag{2.21}$$

where u_d is the characteristic eddy velocity and d is the eddy characteristic length

$$E_\sigma = \sigma A \tag{2.22}$$

the surface energy is proportional to the surface. This surface energy of the drop's system increases as the drop splits into smaller drops the volume of which have to be equal to the volume of the initial one.

In order to picture better the how the surface energy changes when the single drops splits into smaller drops we can picture it with the following example. The idea is that we have a drop with a volume V which has surface energy σd^2 which splits into two drops of volume V_1 and V_2 which have surface energy σd_1^2 and σd_2^2 respectively. One can check that $\sigma d^2 < \sigma d_1^2 + \sigma d_2^2$.

From the relations energetic equivalences it is found, [1], that the temporal derivative of the surface energy or energy change per unit surface is

$$\partial_t E_\sigma \;=\; \vartheta \;=\; -\sigma n_i S_{ij} n_j \tag{2.23}$$

which denotes that the increment of energy depends on the rate-of-strain and we can search then for how is the temporal evolution of the rate-of-strain using the Navier-Stokes equations, thus finding that the evolution of S_{ij} is dependent on the surface energy. Hence, this shows us that there exists a non-linear relation between the surface energy and velocity gradients, rate-of-strain [1].

2.3.2 Energetics of drop breakup

The study of the energetics of drop breakup has one key takeaway which is what is observed for the energy change per unit surface ϑ depending on the Weber number, which symbolizes the ratio between inertial and surface forces. The analysis is performed in order to observe how the surface energy changes its gradient for two different possible influences. The study differentiates the outer eddies in the simulation and the inner eddies from the drop mostly distributed along the interface and how each contribution changes when the Weber number is increased and thus the inertial forces become less significant in comparison to the surface tension ones.

On the obtained figure 3a we can see that $\vartheta > 0$ at outer eddies and $\vartheta < 0$ for inner eddies for values of We smaller than some We_c such that one could interprets it such that there is an increase of surface energy due to outer eddies while a decrease for inner eddies until a certain point in We where both contributions are positive at which the breakup of the drop becomes faster and easier.

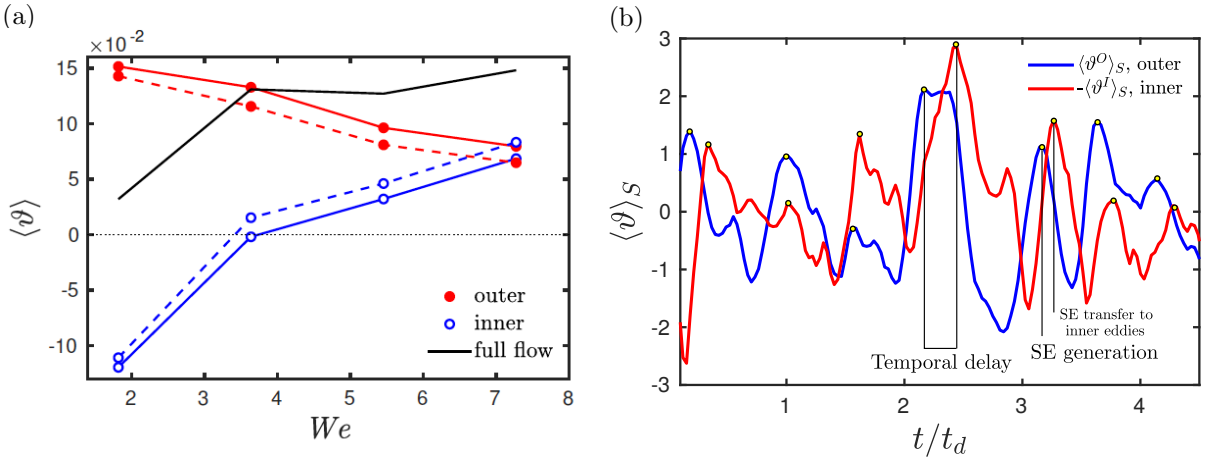

Figure 3: (a) Mean of ϑ as a function of We. (b) Temporal evolution of the free energy change per unit surface of the drop. [1]

Thus we are interested in the $We < We_c$ region in order to better understand the mechanisms that cause a drop to break, but not instantaneously. We consider these temporal evolution energy exchanges to be such that the outer eddies exert a force and pass energy (kinetic) onto the drop's surface which deforms and in order to get to its minimum energy state, exchanges this kinetic energy to its inner fluid feeding in this way turbulence and forming inner eddies.

We also want to give attention to the plot 3b of how the energy change per unit surface evolves in time such that one observes an oscillatory behavior for both inner and outer eddies in a special way. A maximum in the temporal evolution of the contribution of the outer eddies implies a maximum for the inner eddies but with a small delay. This represents the energy exchange between outer and inner eddies where the drop relaxes (gets to the minimum surface energy) transferring this energy onto the outer eddies causing a minimum of the inner eddies when a maximum of the outer happens. This mechanism endures in a repetitive manner until the energy increment is so big that the drop can not dissipate it and breaks.

2.4 Scales in turbulent flow and the energy cascade

Kolmogorov suggested in 1941, [10], that the size of dissipating eddies depends on the parameters that are relevant to the smaller eddies. These parameters are the rate ε at which the energy has to be dissipated by the eddies, and the diffusivity ν that dampens the velocity gradients. Using ε and ν teaches us that the length scale is

$$\eta = (\nu^3/\varepsilon)^{1/4} \tag{2.24}$$

which is called the Kolmogorov microscale. Therefore a decrease of ν only decreases the scale at which viscous dissipation takes place, and not the dissipation rate ε.

Now the rate at which kinematic energy dissipates in a fluid is $\varepsilon = 2\nu S_{ij}S_{ij}$ per unit mass, where S_{ij} is the rate-of-strain tensor. Therefore dissipation is particularly pronounced in regions where the instantaneous velocity gradient, and consequently the shear stress, is large. This suggests that the dissipation of mechanical energy within a turbulent flow is concentrated in the smallest eddies.

The dissipation rate ε is an extremely important quantity that controls the flow of energy from the large scales where it is injected to the small scales where it is dissipated by viscosity. This progressive energy cascade scheme from larger to smaller eddies was immortalized by Richardson (1922).

Richardson's energy cascade idea is as follows: larger eddies, which are normally created the forcing mechanism of turbulence, are themselves subjected to inertial forces and will quickly 'break-up' and pass their energy to even smaller eddies. In fact, the life expectancy of a typical eddy is rather short, on the order of so-called turn-over time (l/u). Of course, the smaller eddies are themselves transient and in return pass their energy to even smaller structures, and so on.

Therefore, at every instant, there is a continuous cascade of energy from the large scales to the small ones. Crucially viscosity plays no role in this cascade. That is, since $Re = ul/\nu$ is large, the viscous stresses acting on large eddies are negligible. This is also true for their offspring, the whole process is essentially driven by inertial forces. The cascade comes to a pause however when the size of the eddy becomes so small that Re, based on the size of the smallest eddies, is on the order of unity. Up to this point dissipation becomes significant when viscous forces become important. Energy is destroyed only in the later stages of the process, when the structures are so fine that Re, based on small-scale structures, is of the order of unity. In this sense, viscosity plays a rather passive role, trapping any cascade of energy from below from above.

Let u and v represent typical velocities associated with the largest and smallest eddies respectively. Also, let l and η be the length scales of the largest and smallest eddies. We now know that eddies pass most of their energy to smaller structures on a timescale of their turnover time, and therefore the rate at which energy (per unit mass) is passed down the energy cascade. of the biggest eddies

$$\Pi \sim u^2/(l/u) = u^3/l \tag{2.25}$$

When conditions are statistically stationary this magnitude must be exactly equivalent to the energy dissipation rate on the smallest scales. If not, then an accumulation of energy would occur on the intermediate scale, and this possibility is excluded in the explanation because we want the statistical structure of the turbulence to be the same from one moment to the next. The energy dissipation rate in smaller eddies is of the order of $\varepsilon \sim \nu S_{ij} S_{ij}$ where S_{ij} is the rate-of-strain associated with eddies smaller, $S_{ij} \sim v/\eta$. This gives $\varepsilon \sim \nu(v^2/\eta^2)$, since the dissipation of the turbulence energy, ε, must be equal to the rate at which the energy enters the cascade Π, we have

$$u^3/l \sim \nu(v^2/\eta^2) \tag{2.26}$$

recovering that Re that is based on v and η is of the order of unity ($v\eta/\nu \sim 1$) and combining the expressions we obtain

$$\eta \sim l\, Re^{-3/4} = (\nu^3/\varepsilon)^{1/4} \tag{2.27}$$

$$v \sim u\, Re^{-1/4} = (\nu\varepsilon)^{1/4} \tag{2.28}$$

This scales η and v are called the Kolmogorov microscales of turbulence, while l is called the integral scale [7].

2.5 Study of invariants of velocity gradient related tensors

In the study of turbulent flows we find an intrinsic difficulty when it comes to conceptually visualizing three dimensional steady and unsteady flow patterns. This is why the use of critical point concepts to describe flow patterns provides a framework and a methodology for overcoming these difficulties [11]. Critical point theory (also known as "phase plane" or "phase space" theory) has been widely used to examine solutions of autonomous ordinary differential equations in many fields of physics [12].

A critical point is a point in the flow where all three components of velocity are zero relative to an appropriate observer and therefore the slope of the streamline is indeterminate. Asymptotically exact solutions of the Navier-Stokes equations can be derived near the critical points, and these give a series of standard flow patterns [13].

In the past, topologies derived from critical points in three-dimensional flows have been examined using simple two-dimensional phase-plane analysis. The methodology used in different studies, and that has been chosen for our case, makes use of the fact that in three dimensions there are planes (called eigenvector planes) that contain certain solution trajectories.

Starting from the consideration of each one of the eigenvectors, in return the velocity field is expressed as a set of linearlized Taylor series expansions that make use of 2x2 matrices

[14]. These matrices have two invariants, p and q, and these invariants are used to define various types of critical points.

The planes of the eigenvectors in many of the previously studied cases were easily identified and located, particularly if there were planes of symmetry involved or if a solid surface was specified as a boundary condition in the flow pattern. In the most general case, these characteristics that simplify the problem are not present, and therefore it becomes important to use an analysis based on three invariants of a 3x3 tensor to be able to identify the planes of the eigenvectors. These three invariants are sufficient to fully classify any flow pattern topology in three dimensions.

The set of three first-order differential equations can be written as

$$\begin{pmatrix} \dot{x}_1 \\ \dot{x}_2 \\ \dot{x}_3 \end{pmatrix} = \begin{pmatrix} a_{11} & a_{12} & a_{13} \\ a_{21} & a_{22} & a_{23} \\ a_{31} & a_{32} & a_{33} \end{pmatrix} \begin{pmatrix} x_1 \\ x_2 \\ x_3 \end{pmatrix} \tag{2.29}$$

where a_{ij} are real constants. In the case of a fluid flow the a_{ij} are the elements velocity gradient or rate-of-deformation tensor $\partial \dot{x}_i / \partial x_j$ evaluated at (x_1, x_2, x_3). If the flow is unsteady, which is our case of study, then solution trajectories correspond to particle paths.

The eigenvalues of $\boldsymbol{A}$ are λ_1, λ_2 and λ_3 and therefore it follows

$$[\boldsymbol{A} - \lambda_i \mathbb{1}] \, \vec{e}_i \, = \, 0 \tag{2.30}$$

where $\vec{e}$ is the corresponding eigenvector. The eigenvectors can be determined by solving the characteristic equation, which for a 3x3 matrix can be written as

$$det(\boldsymbol{A} - \lambda_i \mathbb{1}) \, = \, \lambda_i^3 + P\lambda_i^2 + Q\lambda_i + R \, = \, 0 \tag{2.31}$$

where

$$P \, = \, -(a_{11} + a_{22} + a_{33}) = -tr \, [\boldsymbol{A}] = 0 \tag{2.32}$$

by the incompressibility condition,

$$Q \, = \, \begin{vmatrix} a_{11} & a_{12} \\ a_{21} & a_{22} \end{vmatrix} + \begin{vmatrix} a_{11} & a_{13} \\ a_{31} & a_{33} \end{vmatrix} + \begin{vmatrix} a_{22} & a_{23} \\ a_{32} & a_{33} \end{vmatrix} = \frac{1}{2}(P^2 - tr \left[\boldsymbol{A}^2 \right]) = -\frac{1}{2} \, tr \left[\boldsymbol{A}^2 \right] \tag{2.33}$$

and

$$R \, = \, \begin{vmatrix} a_{11} & a_{12} & a_{13} \\ a_{21} & a_{22} & a_{23} \\ a_{31} & a_{32} & a_{33} \end{vmatrix} = -det \, [\boldsymbol{A}] = \frac{1}{3}(-P^3 + 3PQ - tr \left[\boldsymbol{A}^3 \right]) = -\frac{1}{3} \, tr \left[\boldsymbol{A}^3 \right] \tag{2.34}$$

which are the first, second and third invariants of the velocity gradient tensor respectively.

This approach to the study of the velocity gradient in turbulent flow from the investigation of its second and third invariants i.e. Q and R respectively, is known as topological methodology [11].

Let the rate-of-deformation of velocity gradient tensor ($A_{ij} = \partial \dot{x}_i / \partial x_j$) be broken up into a symmetric and antisymmetric (or skew-symmetric) component

$$A_{ij} = S_{ij} + W_{ij} \tag{2.35}$$

where $S_{ij} = (\partial \dot{x}_i / \partial x_j + \partial \dot{x}_j / \partial x_i)/2$ is the symmetric tensor or rate of strain tensor which we previously already introduced and explained, and $W_{ij} = (\partial \dot{x}_i / \partial x_j - \partial \dot{x}_j / \partial x_i)/2$ the skew-symmetric or rate-of-rotation tensor.

In a similar way to the previous definition of the three invariants of A_{ij}, one can define in an equivalent way the three invariants for the symmetric tensor S_{ij} (P_S, Q_S, R_S) and three corresponding to the antisymmetric W_{ij} (P_W, Q_W, R_W) that are defined by their respective characteristic equations. It should be noted that $P_S = P_W = P_A = 0$ in addition to $R_W = 0$. If the previous steps are done it can also be shown that Q_S is negative definite while Q_W is positive definite.

There are different reasons for studying the invariants of the velocity gradient tensor. The first is because working with invariants means that the results obtained are invariant with respect to the coordinates (invariant with respect to an affine transformation). Furthermore, the invariants of the velocity gradient are independent of the frame of reference of a moving observer (Galilean invariance). Second, in the case of an incompressible fluid for which the first invariant is zero (our case study), the three-dimensional field collapses into a compact region of a two-dimensional space. And finally, turbulent flows are characterized by a wide range of scales that we want to study [15, 16, 17].

In relation to this, we know that relatively small velocity gradients of the order of U/δ occur on large scales, and much larger velocity gradients of the order of $U/\delta(R_\delta)^{1/2}$ occur on smaller scales. The quantities U and δ are the integral velocity and length scales and R_δ is the Reynolds number of the flow. The distribution of the different length scales in the different regions of the invariant figures makes it easy to identify general topological characteristics at different scales.

To finish introducing the study of the velocity gradient invariants, it is necessary to explain how the plots are constructed to visualize the features that these invariants describe. The invariant plot method for analyzing flow fields was introduced by Chen *et.al.* [18]. The procedure for the construction of the plots can be summarized with the following points: (i) the nine derivatives of the velocity gradient tensor are evaluated at each point of the computed field, (ii) the invariants (Q, R) and of the other tensors of interest are determined at each point, (iii) the resulting pairs of the phase-plane (Q, R) are cross-plotted resulting in a scatter plot.

In practice, while scatter diagrams are very useful for revealing topological characters of the finer scales of motion, which are characterized by the largest gradients of the flow, the lower gradients of motion that characterize large or intermediate scales are observed by superimposing layers and layers of dots.

To solve this, these scatter diagrams are replaced by contour diagrams of the number of density of points (joint probability distribution function) that belong within an area of the invariant space. These diagrams are essentially equivalent to unnormalized diagrams

of joint probability distribution functions. Due to extreme variations in the number of densities that occur, the levels of the contour diagram are chosen based on the number of points that each level we want to contain. This is done in order to ensure that the isolated points are captured in such a way that the properties of the scatter diagram are preserved far from the origin, while providing information on the distribution of the invariants near the origin which they correspond to large and intermediate scales of motion.

So that later the comprehension of the plots is more clear, it is now necessary to explain what is the physical meaning of each of the invariants of interest, what each invariant measures. For this, if the previous expressions are developed for each component of the tensor, an equivalent expression can be obtained with the vorticity and the rate-of-strain [19, 7].

For the invariants derived from the strain tensor or the velocity gradient tensor we have the following.

$$Q_A = -\frac{1}{2} tr\left[\boldsymbol{A}^2\right] = -\frac{1}{2} S_{ij} S_{ij} + \frac{1}{4} \omega_i \omega_i \tag{2.36}$$

$$R_A = -\frac{1}{3} tr\left[\boldsymbol{A}^3\right] = -\frac{1}{3} (S_{ij} S_{jk} S_{ki} + \frac{3}{4} \omega_i S_{ij} \omega_j) \tag{2.37}$$

The second invariant we can see that it has the sum of the product of the strain rate that symbolizes the intensity of the strain field and the second component the square of the vorticity and therefore the intensity of the field of this. For the third invariant it is the sum of the strain to the cube that symbolizes the self-amplification of the strain, that is, the production of the strain as a result of self interactions as a feedback mechanism that causes the regions of the strain field to become even more intense. The second term that combines the vorticity with the strain field symbolizes the vortex stretching.

In the case of the invariants of the rate-of-strain tensor they are simpler,

$$Q_S = -\frac{1}{2} S_{ij} S_{ij} \tag{2.38}$$

$$R_S = -\frac{1}{3} S_{ij} S_{jk} S_{ki} \tag{2.39}$$

the second tensor symbolizes the intensity of the field and the third its self-amplification. And for the skew-symmetric component we can see that the second invariant is the intensity of the vorticity.

$$Q_W = \frac{1}{4} \omega_i \omega_i \tag{2.40}$$

It should be noted that in this case the third invariant is zero, as are the first invariants of each of the tensors.

3 Study of magnitude of velocity gradients of the flow

Once all these theoretical concepts are established, we perform a first analysis on the velocity gradient related magnitudes, vorticity and rate-of-strain, to observe how its magnitudes changes with respect to the distance to the interface of the drop. The magnitude of the fields is given by the square of these gradients, since it measures the strength of the vorticity and rate-of-strain fields without a vector implication, which are calculated from the velocity field at all points in the flow.

After calculating the square of the vorticity and strain tensor at all points, we do the analysis for different regions considering these fields at different distances from the drop interface as a reference point, which will be our zero. Therefore we will define the intensity of the vorticity at a distance from the interface as

$$\boldsymbol{\omega}' = G(\boldsymbol{x};\Delta)\,\boldsymbol{\omega} \tag{3.1}$$

where $G(\boldsymbol{x};\Delta)$ is defined by

$$\begin{aligned} G(\boldsymbol{x};\Delta) &= 1 \text{ if } |\boldsymbol{x}-\boldsymbol{x}_s| < \Delta \text{ and } \boldsymbol{x} \in O \\ G(\boldsymbol{x};\Delta) &= 0 \text{ if otherwise.} \end{aligned} \tag{3.2}$$

G is the mask that defines the points of the field that we want to take according to the distance they are from the interface. x_s represents the coordinates of the surface and O represents all the points of the flow which lay outside the drop. In the same way, a mask can be defined for the case of the interior of the drop.

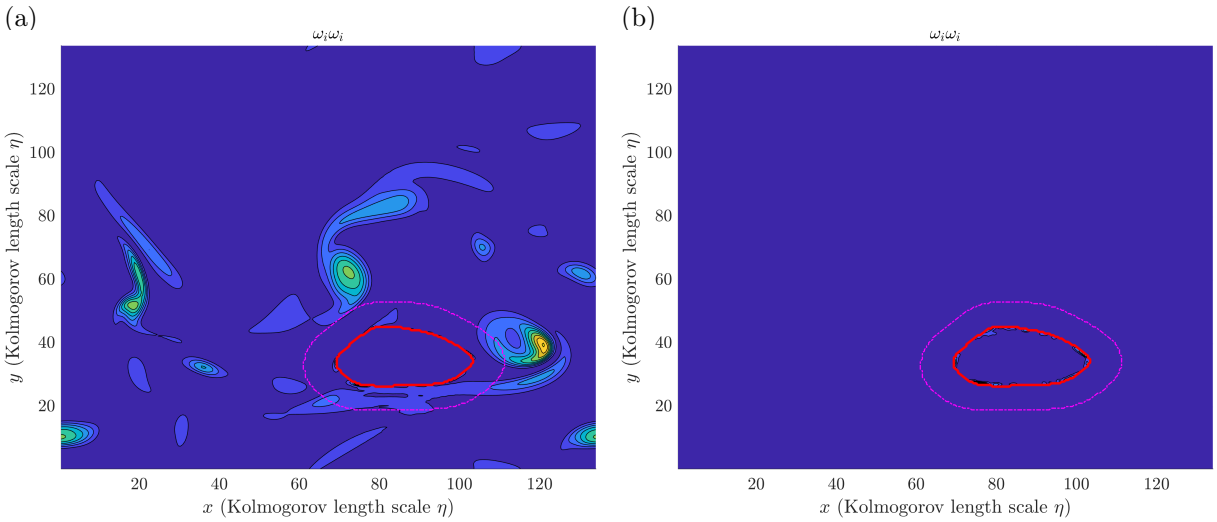

Figure 4: Vorticity to the square for (a) the outside of the drop and (b) the inside of the drop. The red line represents the interface of the drop and the magenta dotted is at a distance $\Delta \sim 6.67\eta$ from the interface of the drop.

To obtain the magnitude of the gradients at the different distances with respect to the interface of the drop, we use the definition of the mask to obtain consecutive sections of the flow, which we achieve by superimposing two masks with Δ and $\Delta + \delta\Delta$, that is, with different distances from the interface of the drop. As we can see in 4, the desired section is between the red line and the magenta dashed line, in this region is where we calculate the

square of the gradients and we average the points to have a mean value of the magnitude of vorticity and rate-of-strain. We repeat this process for consecutive sections outward and inward of the drop with a section width of $\delta\Delta \sim 1.67\eta$.

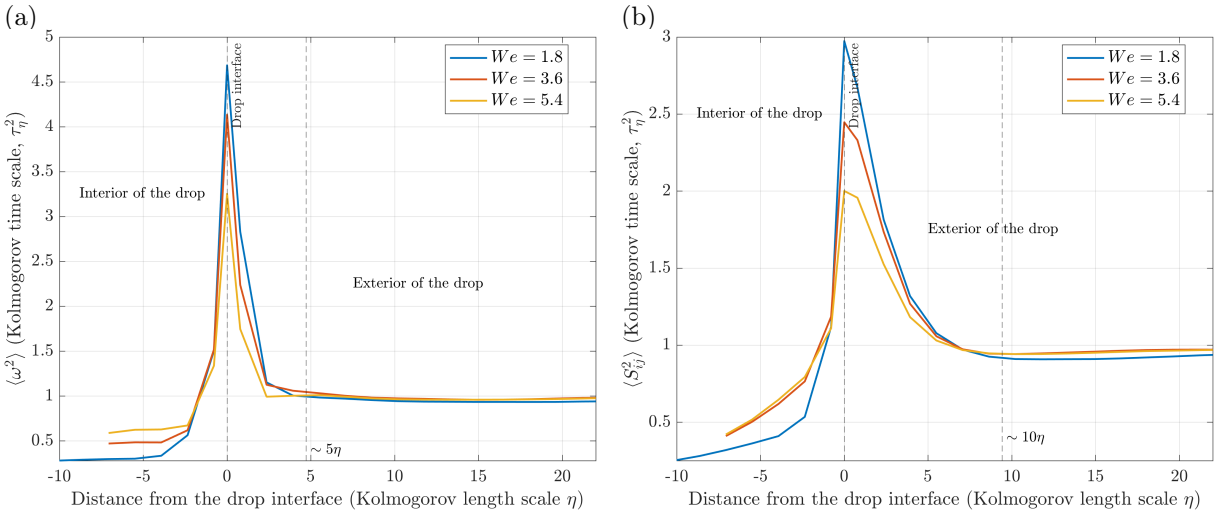

Figure 5: (a,b) average of the magnitude of the (a) the vorticity field and (b) the rate-of-strain tensor of the flow field at different distances from the interface of the drop.

The result of the analysis of the mean of the square of the vorticity and the strain tensor for different Weber numbers at different distances to the drop's interface is given at figure 5. It is observed in both cases that there is a nominal value both inside and outside the drop and as we get closer to the drop there is a substantial increase up to the interface of the drop where there is a maximum that increases as the Weber number decreases. The maxima in the gradients occurs at the interface because the mechanism for producing the gradients in this case is not only turbulence, but also the surface tension of the drop that occurs at the interface of the drop. This results in a maxima of the gradients which varies depending on the Weber number, since the adimensional number regulates the interplay between surface and kinetic forces, and for lower Weber number the surface forces are more dominant and therefore the maximum has a greater magnitude.

To present the plot, we have normalized the distance with respect to the Kolmogorov length scale and the gradients with the Kolmogorov time scale, both Kolmogorov scales are defined from the characteristics scales of small eddies as explained in 2.4.

One of the key aspects to emphasize in this first analysis is that the vorticity and the rate-of-strain decay outside the drop to an asymptotic value of one in a different spatial range. Resulting in the fact that, at a certain distance from the drop interface, there is no longer influence of the drop surface dynamics on the average turbulent flow. Therefore we take the distance at which the dynamics of the drop surface no longer has effect on the outside flow the limit range of the strain tensor, since it is the largest. This distance is $\sim 10\eta$ which agrees with study of Vela-Martin & Avila [1].

Once we have these first plots and after subsequent checks with the tensor invariants, we decided to perform the analysis of invariants on four different regions where the dynamics are appreciably different because of the average value of the gradients shown. As seen in figure 6, the division is done in four regions with respect to the surface of the drop. The

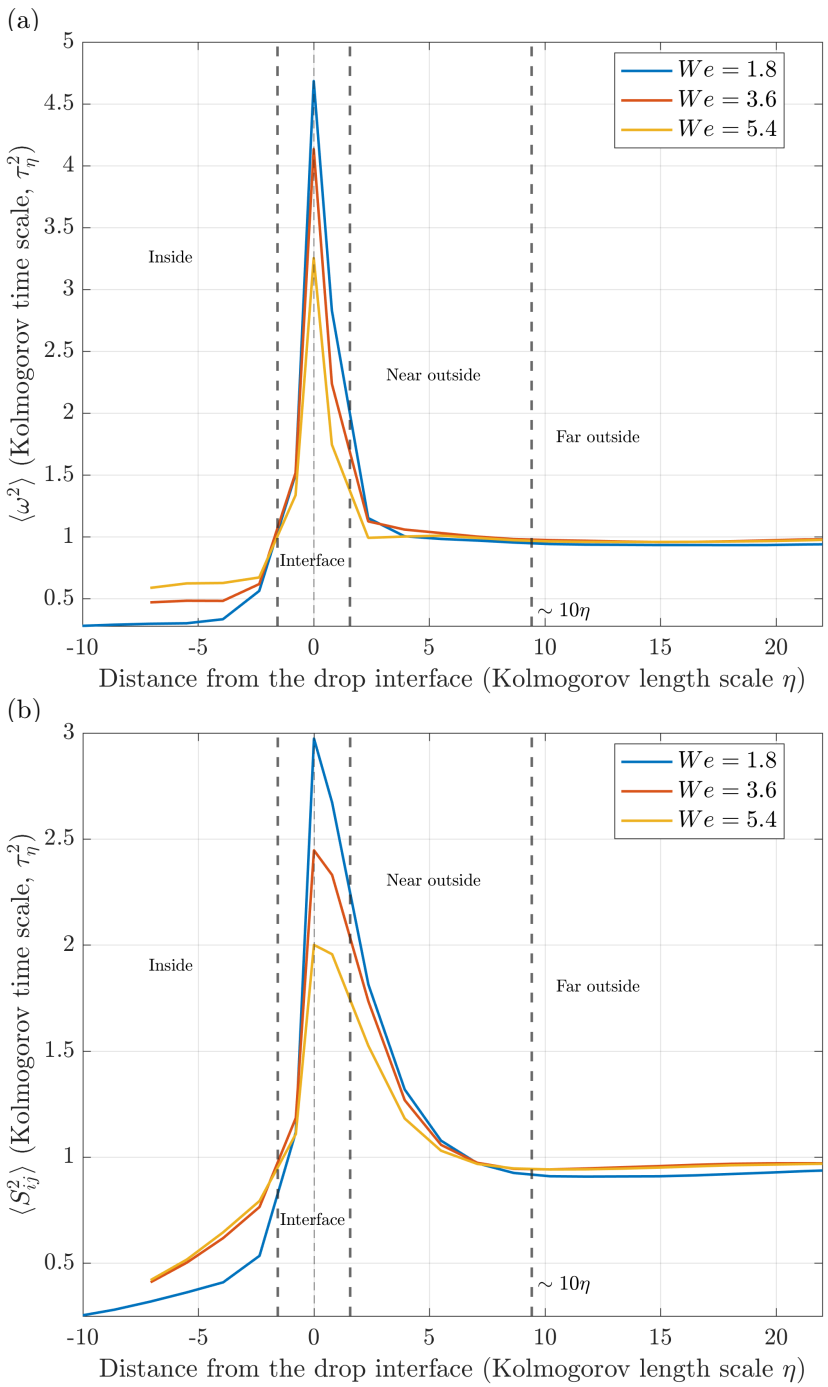

Figure 6: (a,b) average of the magnitude of the (a) the vorticity field and (b) the rate-of-strain tensor of the flow field at different distances from the interface of the drop with vertical lines separating the four regions of interest for the tensor invariant study.

interior region of the drop designated as "inside", the area of the interface of the drop that bears the same name, the area outside the drop but in a range in which it still can be appreciated an influence of the dynamics of the surface of the drop on the turbulent flow, up to the 10η distance, that we will call “near outside”. And finally, the outer region away from the drop, called "far outside", that comprises all the outer points of the simulation cube at least 10η away from the surface.

4 Study of the velocity gradient tensor invariants

4.1 Comparing Weber numbers

We start by showing the contour plots of the invariants R_A, Q_A for different Weber numbers in the region away from the drop at figure 7. This plot can be seen in multiple papers as the representative of an average turbulent flow, some say that it is a universal shape [20, 21], the characteristic shape of "teardrop" where the maximum is at the origin and the points are distributed around in an almost elliptical shape but with a preference of the points for the second and fourth quadrants.

We see that the different cases of Weber number collapse at the same contour levels, as one could expect far outside from the drop, the dynamics of the drop does not influence the flow, and therefore the presence of the drop in the flow, and all the dynamics that accompany it, do not alter the behavior of the turbulence far away from the drop.

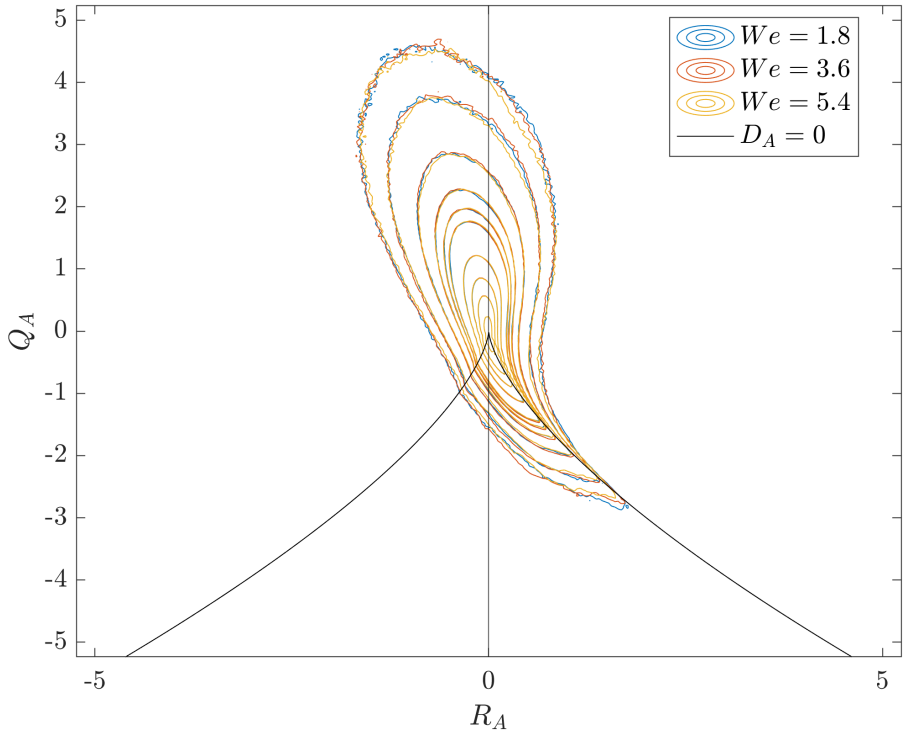

Figure 7: Contour plot of the second and third invariant of the velocity gradient tensor A_{ij} for different Weber numbers at the regions far outside the drop.

As we mentioned before, Q_A gives us the magnitude of the relative intensity of the vorticity and the rate-of-strain. The large negative values indicate regions of strong strain and little vorticity and large positive ones regions of intense enstrophy and therefore dominance of vorticity. For large values of Q_A then $R_A \sim \omega_i S_{ij} \omega_j$ and positive values of R_A symbolize vortex stretching and negative ones vortex compression. For the case when Q_A has large negative values $R_A \sim S_{ij} S_{jk} S_{ki}$, and looking at the plot of figure 7 for positive values of R_A where the contours stretching along the curve $D_A = 0$, in this area of the plot the rate-of-strain field is strong and therefore $\langle S_{ij} S_{jk} S_{ki} \rangle \gg 0$ which means that the strain self-amplification mechanism acts significantly, so that the intensity of the strain causes the strain field to remain intense. [7, 20].

Next, at figure 8, we observe plots of simulations for different Weber numbers comparing the region inside the drop and far outside the drop, we see differences that may indicate differences in the flow dynamics. It can clearly be observed that inside the drop there is less intensity of the vorticity field for smaller Weber numbers.

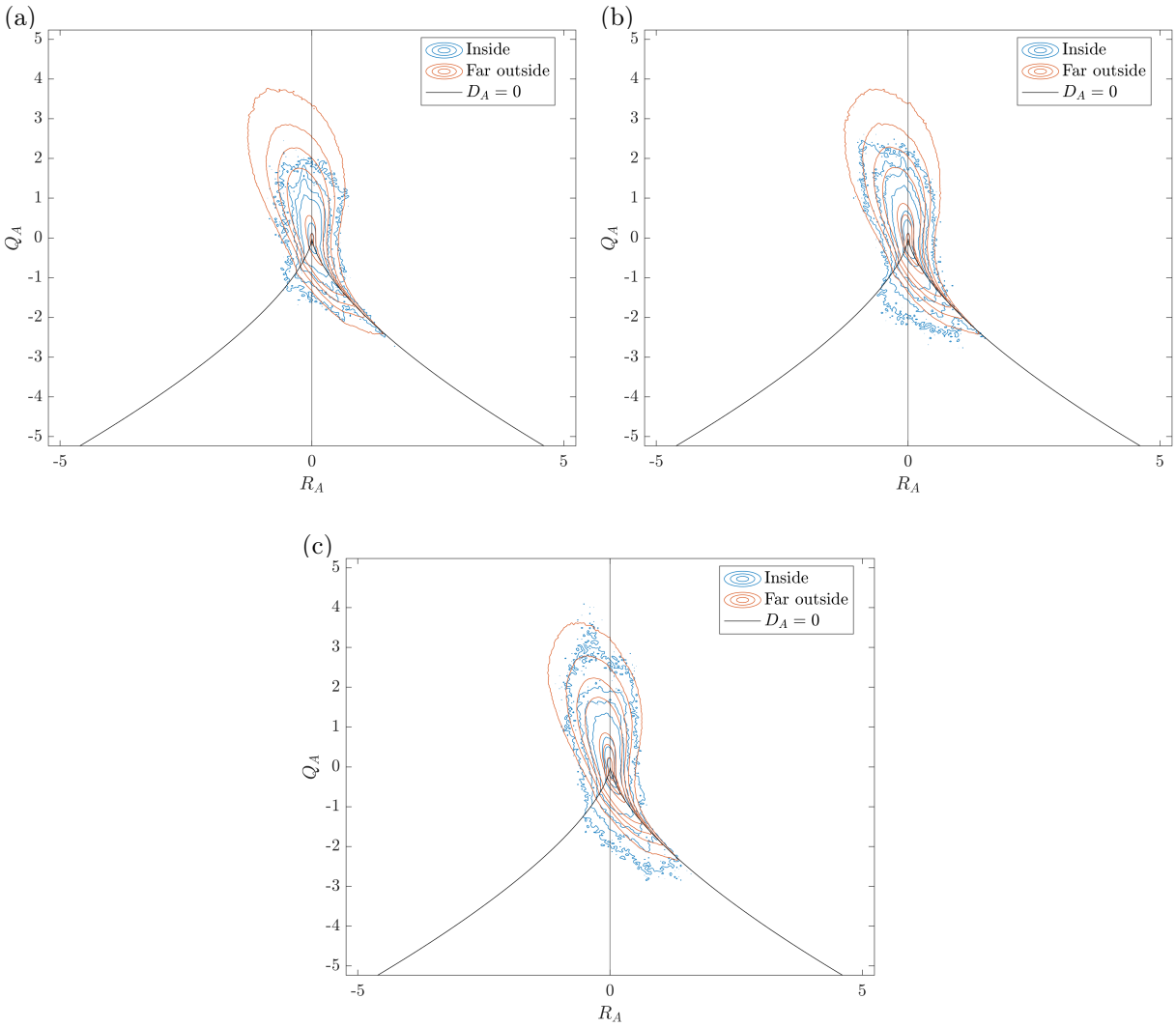

Figure 8: Contour plots of the second and third invariant of the velocity gradient tensor A_{ij} comparing the contours at the inside and far outside region of the drop for Weber numbers (a) $We = 1.8$, (b) $We = 3.6$ and (c) $We = 5.4$.

For 8a the region of $Q_A > 0$ is almost symmetric while we still see that for negative values the contours embrace the curve $D_A = 0$ which indicates that the self-amplification of the strain is still present. The symmetry for the region of vorticity dominance may indicate that inside the drop, intense vorticity can not be stretched into elongated structures that do not fit, which prevents intense vorticity events. Outside, the vorticity can be stretched freely, leading to intense events, because of the predominance of inertial forces. Therefore for the larger Weber number, as can be seen in at 8c, as the inertial forces exceed the surface forces, the dynamics inside the drop get more similar to the turbulent flow outside.

The next plots to examine are in which we compare the interface region of the drop with

far outside the drop, this for different Weber numbers at figure 9. For the case of the invariants in the interface, again we see some differences in the structure of the contours with respect to the average turbulent flow, although we do not see a difference between the simulated Weber numbers. In the interface we see that although we still have a

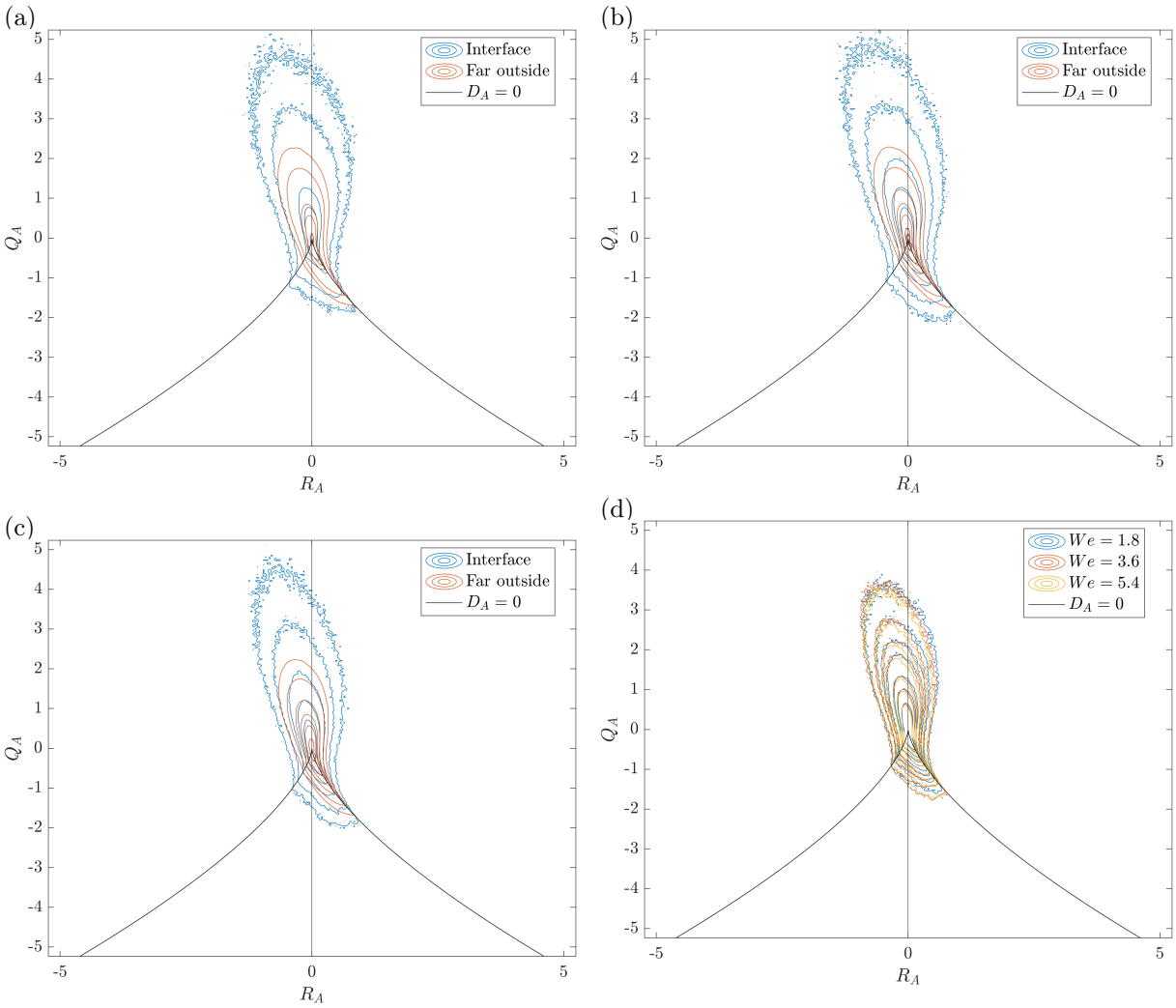

Figure 9: Contour plots of the second and third invariant of the velocity gradient tensor A_{ij} comparing the contours at the interface of the drop and at the far outside of the drop for Weber numbers (a) $We = 1.8$, (b) $We = 3.6$ and (c) $We = 5.4$, and (d) comparing the different Weber numbers only for the interface region.

preference for the second quadrant where $Q_A > 0$ and $R_A < 0$ this time there are not so many points stretching along the zero discriminant curve, which means less importance of the mechanism of strain self-amplification. Despite this, the major observation is the fact that the relationship between inertial forces and surface tension influence in the dynamics of the drop interface cannot be appreciated in an obvious way from the invariants, at least in this range of Weber numbers.

To try to elucidate what happens in the interface more clearly and to confirm if there are differences in the mechanisms of gradient production, we show the invariants of the tensor rate-of-strain.

The following plots at figure 10 are the contours of the pair of rate-of-strain tensor invariants, so that we only analyze the dynamics of the rate-of-strain without the vorticity. In this case we compare again between the interface and the far outside the drop. For this plots again we see a substantial difference with regard to the mechanisms that influence the dynamics of the systems. We see that for the interface the contour of the invariants are almost symmetric with respect to R_S, while for far outside from the drop the points embrace the zero discriminant for positive value of the third invariant, indicating that most flow regions are stretched in two orthogonal directions and contracted in the third. The results of the plots indicate that at the interface there is a reduced self-amplification of the strain, although the gradients are large, in fact the intensity of the strain field is greater at the interface than at the far outside from the drop. Also, no changes are seen according to the Weber number, only maybe in 9d where we observe that the symmetry is more pronounced for smaller Weber values as well as with larger magnitude of strain. The effect of the Weber number on the mechanisms that affect the dynamics of the interface, from the analysis of the invariants, is still inconclusive.

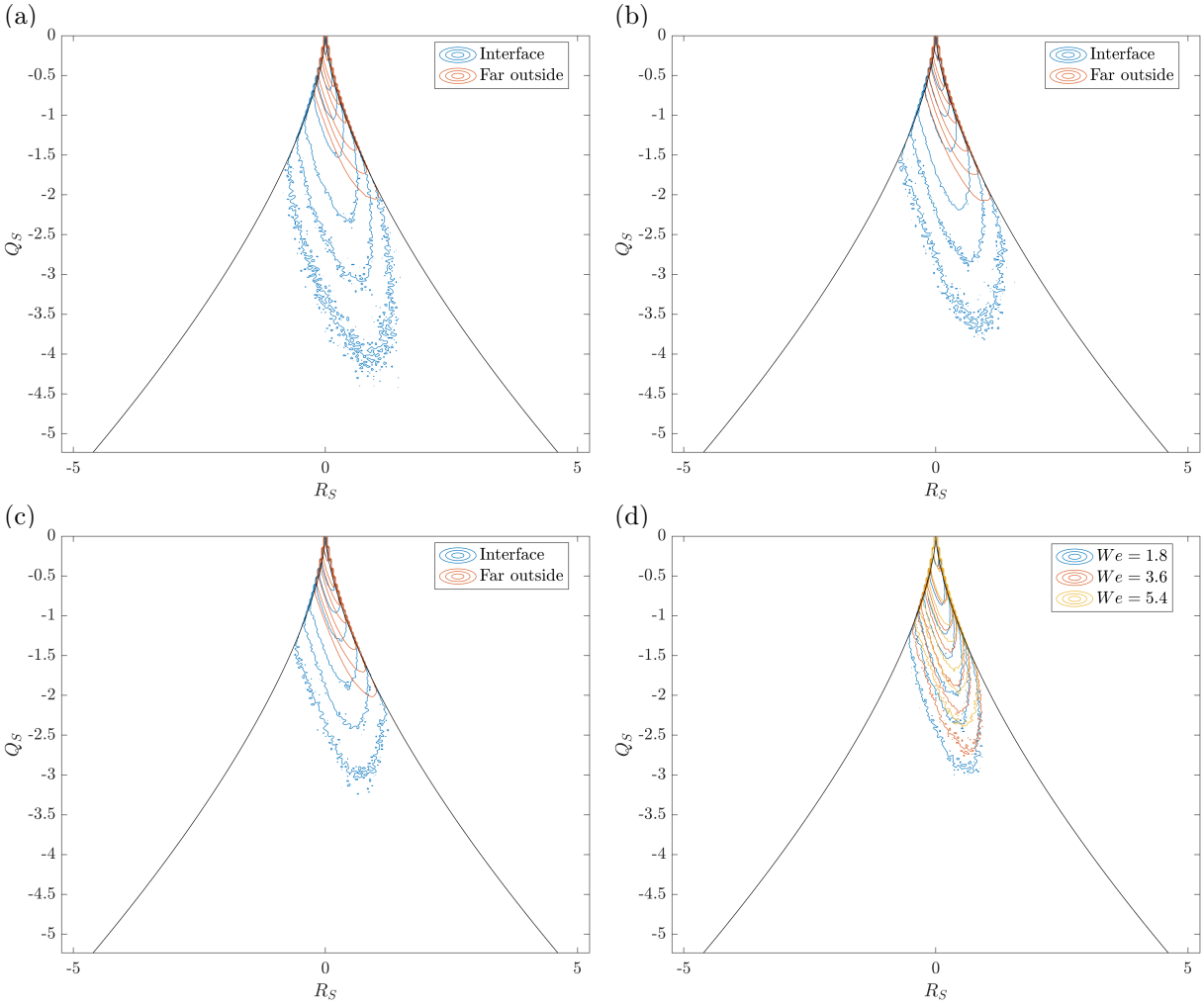

Figure 10: Contour plots of the second and third invariant of the rate-of-strain tensor S_{ij} comparing the contours at the interface of the drop and at the far outside of the drop for Weber numbers (a) $We = 1.8$, (b) $We = 3.6$ and (c) $We = 5.4$, and (d) comparing the different Weber numbers only for the interface region.

4.2 Comparing Viscosities

From here we focus the analysis on what is the central point of the work, the study of the invariants according to the viscosity of the drop. The parameter with which we refer to the viscosity is λ_ν, which gives the relationship between the viscosity of the fluid that makes up the drop and that of the exterior turbulent flow. We consider two cases: one in which the viscosity is the same for both, and another where the viscosity of the drop is four times that of the outside flow.

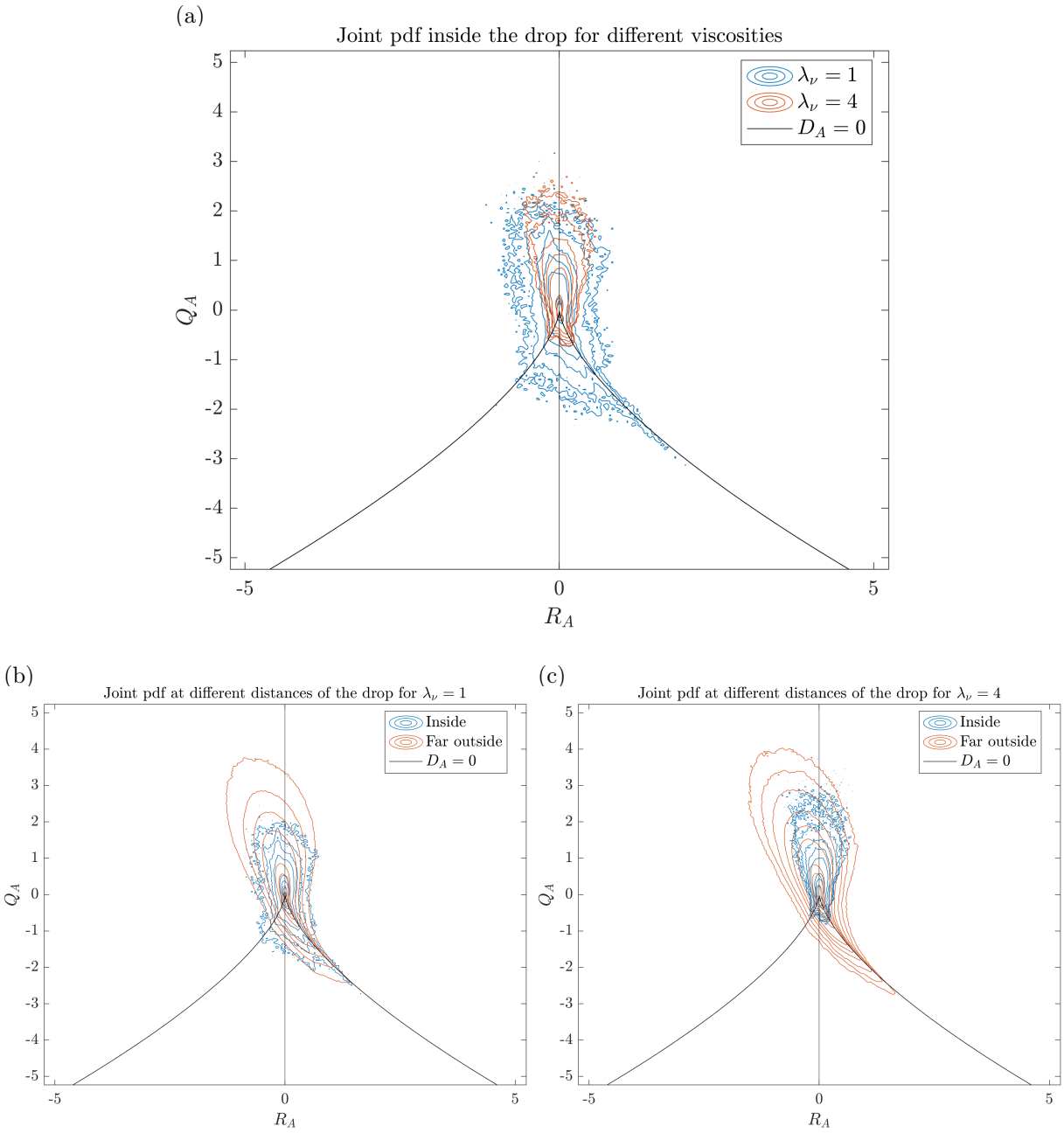

Figure 11: Contour plots of the second and third invariant of the velocity gradient tensor A_{ij} comparing the contours (a) inside the drop and for different viscosities $\lambda_\nu = 1$ and $\lambda_\nu = 4$, (b) the inside and far outside region of the drop for viscosity $\lambda_\nu = 1$ and (c) the inside and far outside region of the drop for viscosity $\lambda_\nu = 4$.

The most important and significant result is the one shown in the figure 11a, where we can see the invariants corresponding to the tensor of the velocity gradient A_{ij} inside the drop for different viscosities. Clear differences can be observed.

For the case of viscosity relation one, the structure of the contours has for a teardrop similar shape and negative values of Q_A have a predominance to stretch along the discriminant zero for positive values R_A, which means that the strain self-amplification mechanism is present, as we can see for a average turbulent flow. In fact, at 11b one can see that both inside and far outside the drop they have a more or less a similar structure of the invariants.

While for the viscosity four times greater than the drop, λ_ν, there is a clear symmetry with respect to the R_A axis, with strain field values also much smaller than the λ_ν case at 11a or outside the drop at 11c. This symmetry indicates that if we make the integral of the strain to the cube ($S_{ij}S_{jk}S_{ki}$) it would give us zero. This means that there is no strain self-amplification inside the drop, even though there is a intense strain field. Thus, there is no turbulence self-amplification inside the drop.

This difference in symmetry of both cases of viscosity can be observed even better in 11b and 11c in which we compare the joint pdf between the inside of the drop and the far outside for the different viscosities.

The next plots to show are those of the figure 12 where it compares different viscosities for the area of the interface of the drop in 12a, and we compare the interface with far outside the drop in 12b and 12c.

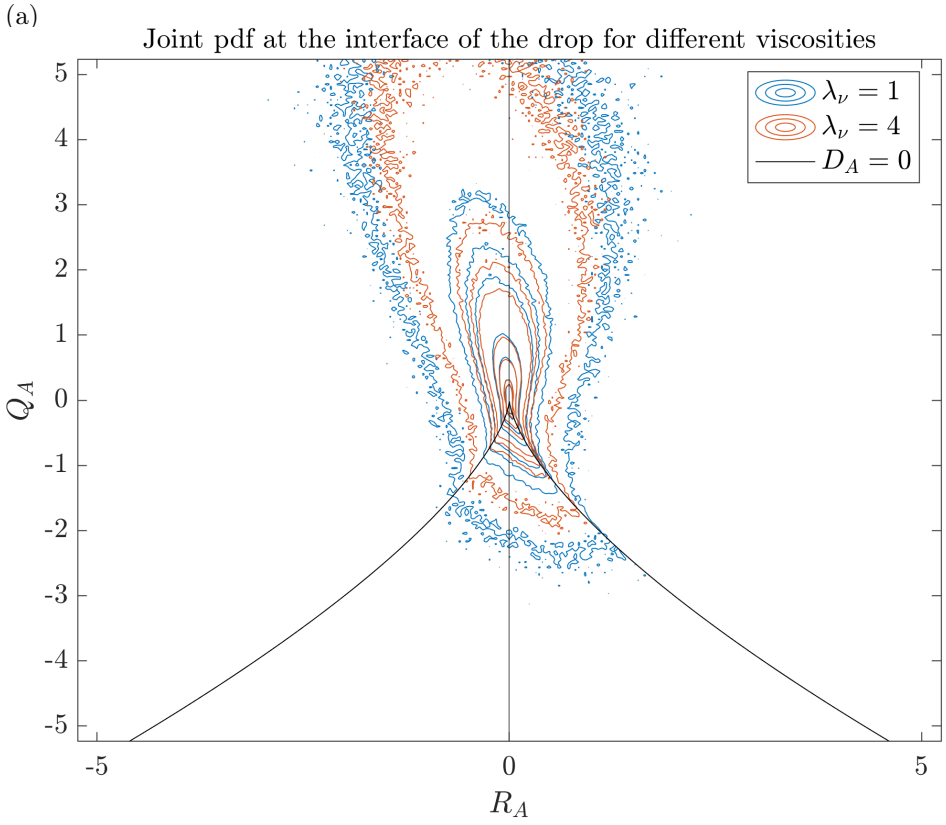

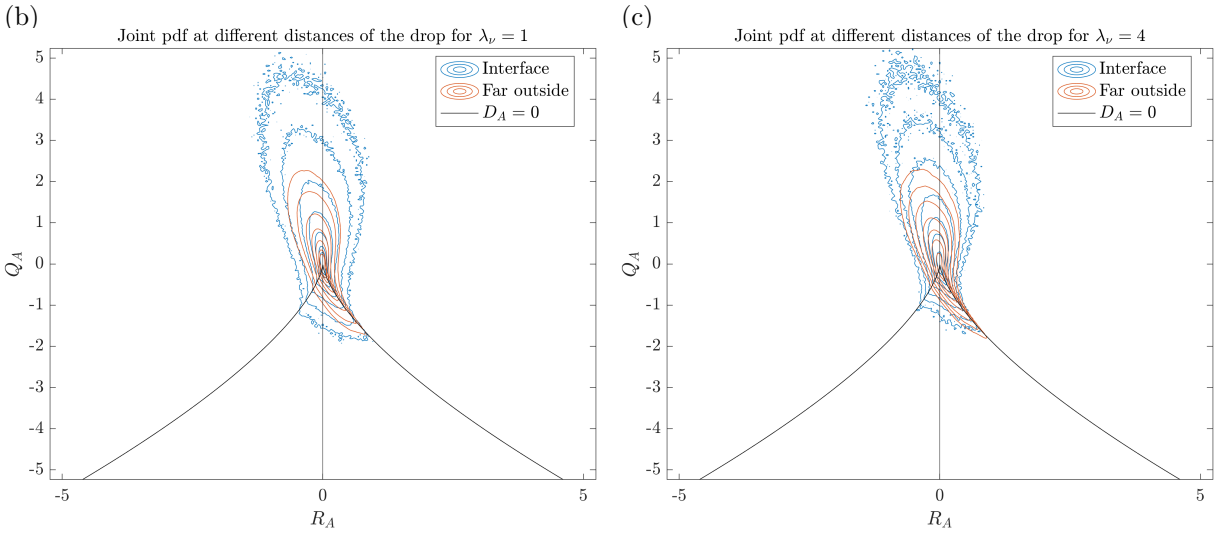

Figure 12: Contour plots of the second and third invariant of the velocity gradient tensor A_{ij} comparing the contours (a) at the interface of the drop and for different viscosities $\lambda_\nu = 1$ and $\lambda_\nu = 4$, (b) the interface and far outside region of the drop for viscosity $\lambda_\nu = 1$ and (c) the interface and far outside region of the drop for viscosity $\lambda_\nu = 4$.

In this case, first in 12a we observe that changing the viscosity of the drop with respect to the external flow does not change the structure of the invariants, which means that the same mechanisms interact in the dynamics of the interface regardless of the viscosity of the drop . The dynamics at the interface depend on the surface tension but not on the viscosity.

We can observe this again in the plots 12b and 12c where, despite the fact that no difference is seen between viscosities, we again see that for the interface there is a less predominance of the strain self-amplification mechanism.

Finally, we show in the figure 13 the diagrams of the invariants for different viscosities between the regions far outside and near outside the drop.

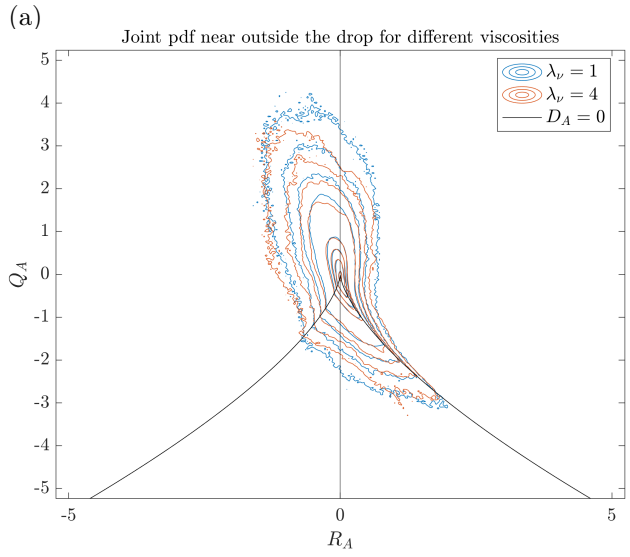

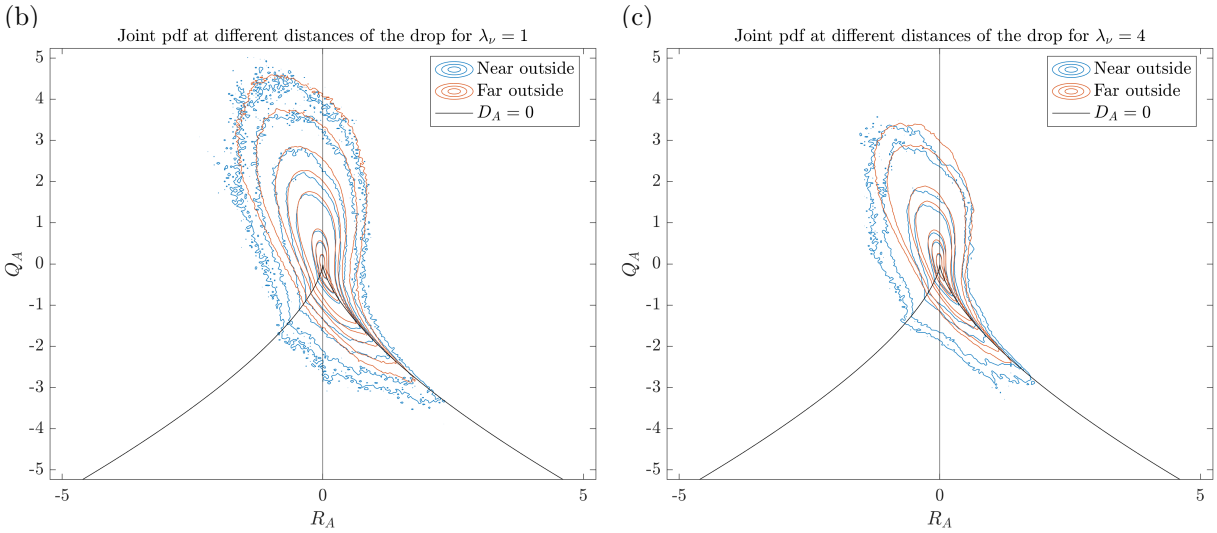

Figure 13: Contour plots of the second and third invariant of the velocity gradient tensor A_{ij} comparing the contours (a) near outside the drop and for different viscosities $\lambda_\nu = 1$ and $\lambda_\nu = 4$, (b) the near and far outside region of the drop for viscosity $\lambda_\nu = 1$ and (c) the near and far outside region of the drop for viscosity $\lambda_\nu = 4$.

In these graphs we could say that for the case it is seen that close outside the drop that for negative values of Q_A, that is, for regions of intense strain, we see that it indicates that the vortex compression mechanism appears in the dynamics (negative values of R_A stretching along $D_A = 0$). The problem is that the contours are not fine enough, this is because the regions that are not the far outside of the drop include few points. To solve this, it is necessary to carry out a study with averages of the invariants of more than one hundred fields (up to a thousand different fields) to see if this structure is maintained.

In addition, it can be observed that for the different viscosities the plots practically collapse, that is, the viscosity does not influence the dynamics of the external flow near the drop. Contours may collapse better by normalizing with a unit that takes viscosity into account. We can only speculate about it since we use the Kolmogorov scale to normalize the gradients, and we do not have data for different Reynolds number. This can be seen when observing that for the levels that represent more density of points, the contours are almost equal, while the fewer points the contour represents, the more different and diffuse they are.

5 Conclusions and further research

To finish this report, it is necessary to present the main conclusions of the work, in addition to proposing improvements for the work and elucidating future research.

One of the clear points that we have taken from the analysis of the flow field gradients is that there is a clear range of influence up to which the drop affects the turbulent flow in which it is immerse, this distance is 10η and it coincides with the study of Vela-Martín & Avila [1]. We also see that the turbulence inside and outside the drop have different intensity and structure in addition to different mechanisms that are responsible for maintaining the turbulent flow.

The most striking result is the fact that the invariants of the gradient tensors tell us that even if the viscosity influences the breakup of the drop the mechanisms of the breakup are similar even when we change the viscosity of the drop. The viscosity plays a role in increasing the rate at which the energy dissipates within the drop. This results in a damping of the intensity of the gradients that come from the interface and outside the drop, which is observed in the fact that the vorticity is weaker and there are less vortices inside the drop and get dissipated more efficiently. Inside a drop with a high viscosity the flow relaminarises due the strong dissipation. The mechanisms by which turbulence interacts with the interface, which are relevant to drop breakup, do not change with the viscosity of the drop.

As a last point, it is necessary to comment on possible improvements to the work. Much remains to be done and that it will be done. One of the clearest improvements is regarding the analysis comparing different viscosities, an analysis should be done with a normalization choosing a unit that depends on the viscosity and the Reynolds number, in addition to making a study of the gradients with the number of Reynolds used in the simulation. As for future research, given the great potential of the topic, there are both possible improvements in terms of experimental research and monitoring tools of the experiments carried out, as well as improvements in the models used to make the simulations of drop breakup.

References

[1] Alberto Vela-Martín and Marc Avila. Energetics of drop deformation with application to turbulence. 2021.

[2] Alexandra E. Komrakova. Single drop breakup in turbulent flow. *The Canadian Journal of Chemical Engineering*, 97(10):2727–2739, 2019.

[3] Sebastian Maaß and Matthias Kraume. Determination of breakage rates using single drop experiments. *Chemical Engineering Science*, 70:146–164, 2012. 4th International Conference on Population Balance Modeling.

[4] John E. Swartz and David P. Kessler. Single drop breakup in developing turbulent pipe flow. *AIChE Journal*, 16(2):254–260, 1970.

[5] Kunio Arai, Mikio Konno, Yuichi Matunaga, and Shozaburo Saito. Effect of dispersed-phase viscosity on the maximum stable drop size for breakup in turbulent flow. *Journal of Chemical Engineering of Japan*, 10(4):325–330, 1977.

[6] Basim O. Hasan. Breakage of drops and bubbles in a stirred tank: A review of experimental studies. *Chinese Journal of Chemical Engineering*, 25(6):698–711, 2017.

[7] P. A. Davidson. *Turbulence: an introduction for scientists and engineers*. Oxford University Press, Oxford, UK, 2004.

[8] Marcel Lesieur. *Fluid Mechanics and Its Applications. Turbulence in Fluids*. Springer Netherlands, 2008.

[9] Cohen I.M. Kundu P.K. *Fluid mechanics.* APA, 2004.

[10] Kolmogorov Andrei Nikolaevich. The local structure of turbulence in incompressible viscous fluid for very large reynolds numbers. *Proc. R. Soc. Lond.*, A(434):9–13, 1991.

[11] Jesús Martín, Andrew Ooi, M. S. Chong, and Julio Soria. Dynamics of the velocity gradient tensor invariants in isotropic turbulence. *Physics of Fluids*, 10(9):2336–2346, 1998.

[12] A E Perry and M S Chong. A description of eddying motions and flow patterns using critical-point concepts. *Annual Review of Fluid Mechanics*, 19(1):125–155, 1987.

[13] M. S. Chong, A. E. Perry, and B. J. Cantwell. A general classification of three-dimensional flow fields. *Physics of Fluids A: Fluid Dynamics*, 2(5):765–777, 1990.

[14] Dhawal Buaria, Eberhard Bodenschatz, and Alain Pumir. Vortex stretching and enstrophy production in high reynolds number turbulence. *Phys. Rev. Fluids*, 5:104602, Oct 2020.

[15] J. Soria, R. Sondergaard, B. J. Cantwell, M. S. Chong, and A. E. Perry. A study of the fine-scale motions of incompressible time-developing mixing layers. *Physics of*

Fluids, 6(2):871–884, 1994.

[16] Brian J. Cantwell. On the behavior of velocity gradient tensor invariants in direct numerical simulations of turbulence. *Physics of Fluids A: Fluid Dynamics*, 5(8):2008–2013, 1993.

[17] P. Bechlars and R. D. Sandberg. Evolution of the velocity gradient tensor invariant dynamics in a turbulent boundary layer. *Journal of Fluid Mechanics*, 815:223–242, 2017.

[18] J. Chen, M. S. Chong, J. Soria, R. Sondergaard, A. Perry, M. Rogers, R. Moser, and B. Cantwell. A study of the topology of dissipating motions in direct numerical simulations of time-developing compressible and incompressible mixing layers. 1990.

[19] Carlos B. da Silva and José C. F. Pereira. Invariants of the velocity-gradient, rate-of-strain, and rate-of-rotation tensors across the turbulent/nonturbulent interface in jets. *Physics of Fluids*, 20(5):055101, 2008.

[20] Andrew Ooi, Jesus Martin, Julio Soria, and M. S. Chong. A study of the evolution and characteristics of the invariants of the velocity-gradient tensor in isotropic turbulence. *Journal of Fluid Mechanics*, 381:141–174, 1999.

[21] J. I. Cardesa, D. Mistry, L. Gan, and J. R. Dawson. Invariants of the reduced velocity gradient tensor in turbulent flows. *Journal of Fluid Mechanics*, 716:597–615, 2013.